The Meteoritical Society

Meteoritics & Planetary Science 44, Nr 4, 589–601 (2009)
Abstract available online at http://meteoritics.org

Clastic matrix in EH3 chondrites

Alan E. RUBIN[1*], Christian D. GRISET[2], Byeon-Gak CHOI[1, 3], and John T. WASSON[1, 4]

[1]Institute of Geophysics and Planetary Physics, University of California, Los Angeles, California 90095–1567, USA
[2]Physics Department 103-33, California Institute of Technology, Pasadena, California 91125, USA
[3]Department of Earth Science Education, Seoul National University, Seoul 152-748, Republic of Korea
[4]Department of Earth and Space Sciences and Department of Chemistry and Biochemistry,
University of California, Los Angeles, California 90095, USA
*Corresponding author. E-mail: aerubin@ucla.edu

(Received 18 June 2008; revision accepted 22 January 2009)

Abstract–Patches of clastic matrix (15 to 730 μm in size) constitute 4.9 vol% of EH3 Yamato (Y-) 691 and 11.7 vol% of EH3 Allan Hills (ALH) 81189. Individual patches in Y-691 consist of 1) ~25 vol% relatively coarse opaque grain fragments and polycrystalline assemblages of kamacite, schreibersite, perryite, troilite (some grains with daubréelite exsolution lamellae), niningerite, oldhamite, and caswellsilverite; 2) ~30 vol% relatively coarse silicate grains including enstatite, albitic plagioclase, silica and diopside; and 3) an inferred fine nebular component (~45 vol%) comprised of submicrometer-size grains. Clastic matrix patches in ALH 81189 contain relatively coarse grains of opaques (~20 vol%; kamacite, schreibersite, perryite and troilite) and silicates (~30 vol%; enstatite, silica and forsterite) as well as an inferred fine nebular component (~50 vol%). The O-isotopic composition of clastic matrix in Y-691 is indistinguishable from that of olivine and pyroxene grains in adjacent chondrules; both sets of objects lie on the terrestrial mass-fractionation line on the standard three-isotope graph. Some patches of fine-grained matrix in Y-691 have distinguishable bulk concentrations of Na and K, inferred to be inherited from the solar nebula. Some patches in ALH 81189 differ in their bulk concentrations of Ca, Cr, Mn, and Ni. The average compositions of matrix material in Y-691 and ALH 81189 are similar but not identical—matrix in ALH 81189 is much richer in Mn (0.23 ± 0.05 versus 0.07 ± 0.02 wt%) and appreciably richer in Ni (0.36 ± 0.10 versus 0.18 ± 0.05 wt%) than matrix in Y-691. Each of the two whole-rocks exhibits a petrofabric, probably produced by shock processes on their parent asteroid.

INTRODUCTION

Fine-grained silicate-rich matrix material in anhydrous, unmetamorphosed chondrites is derived mainly from nebular dust. Matrix material was noted previously in type 3 enstatite chondrites (e.g., Kimura 1988; Huss and Lewis 1995; Ebata et al. 2006), but not adequately characterized. Among the most primitive enstatite chondrites (Prinz et al. 1984) are the Antarctic EH3 chondrites Yamato 691 (hereafter Y-691), a single 715 g stone recovered in Queen Maud Land, and Allan Hills A81189 (hereafter ALH 81189), a single 2.6 g stone recovered in Victoria Land.

Y-691 contains abundant well-defined chondrules (Okada et al. 1975, Nagahara 1985, Kimura 1988), some of which contain magnesian olivine phenocrysts (Nagahara 1985) and glassy mesostases (Prinz et al. 1984). (Olivine is absent in the metamorphosed type 5 and 6 enstatite chondrites [e.g., Rubin 1997]). Also present in Y-691 are complex, unrecrystallized metal-sulfide ± silicate assemblages, some of which include grains of graphite, phosphide and silicide (Nagahara 1985; Kimura 1988). Kimura (1988) identified matrix material in Y-691 as consisting of "fine-grained silicate and opaque minerals filling the interstices among fragments and chondrules."

ALH 81189 contains well-defined chondrules and chondrule fragments, some of which have magnesian olivine phenocrysts. Also present are opaque assemblages, grains of silica and polysynthetically twinned low-Ca pyroxene (Score and Mason 1984). Fine-grained clastic matrix material is moderately abundant.

Presolar silicate and carbonaceous grains in Y-691, ALH 81189 and one other EH3 chondrite—Sahara 97072—were identified by Ebata et al. (2006, 2007) and Ebata and Yurimoto (2008). The presolar grains were found within regions of "clastic matrix" as described below.

ANALYTICAL PROCEDURES

We studied thin section Y691,79-1 (Fig. 1a), on loan from the National Institute of Polar Research, Japan, and thin section ALH 81189,7 (Fig. 1b), on loan from NASA Johnson Space Center in Houston. The modal abundances of clastic matrix (see below) in these meteorites were determined microscopically at high magnification (500×) in reflected light using an automated point counter. The UCLA LEO 1430 VP scanning electron microscope (SEM) was used to create backscattered electron (BSE) images of the entire sections of both meteorites using a 15 keV accelerating voltage and a working distance of ~26 mm; in each case, the images were combined into a mosaic. A grid was superposed on the mosaics and used to label the chondrules, matrix patches and other features.

Analysis of the whole-rock petrofabric of Y-691 and ALH 81189 were made using poster-size mosaics of BSE images. In each case, a line was drawn on the poster parallel to the long axis of each non-circular ≥0.5 mm size silicate particle. The angle (i.e., the azimuth) between this line and the vertical (going clockwise) was measured with a protractor. The lengths of longest axis (b) and the longest axis perpendicular to b (i.e., a) were measured for each particle.

The modal abundances of relatively coarse silicate and opaque phases in Y-691 and ALH 81189 were determined by superimposing 17 × 17 square transparent grids (289 points) on BSE images of representative portions of matrix patches—near chondrule J10 for Y-691 and near chondrule D4 for ALH 81189.

Quantitative analytical data for five patches of clastic matrix in Y-691 were obtained by analyzing 49 points in a square ~50 μm × 50 μm grid of each patch; the grid areas had interpoint spacings of 8 to 9 μm. For the five analyzed patches in ALH 81189, the number of points ranged from 28 to 49; in each case the interpoint spacings were 8 μm. Analyses of the clastic matrix patches in both meteorites were made with the JEOL JXA-8200 electron microprobe at UCLA. A 3 μm diameter beam was used to determine 17 elements: O, Na, Mg, Al, Si, P, S, Cl, K, Ca, Ti, Cr, Mn, Fe, Co, Ni, and Zn. (Data for Cl, Ti, Co, and Zn were excluded from the tables because most analyses are below the detection limit.)

Natural and synthetic standards were employed; the beam current was limited to 15 nA to minimize loss of volatiles. Cobalt values were corrected for the contribution of the Fe-Kβ peak to the Co-Kα peak. An analogous procedure for a set of 10 elements was used by Wasson and Rubin (2009) on patches of matrix material in the LAP 02342 CR2 chondrite. In that study, duplicate runs of the same matrix grid areas yielded statistically indistinguishable compositions.

The oxygen-isotopic compositions of five patches of clastic matrix and of olivine and pyroxene grains in adjacent chondrules in Y-691 were measured using the Cameca IMS 7f GEO secondary ion mass spectrometer (SIMS) at the California Institute of Technology. A defocused Cs^+ beam with an intensity of ~2 nA and a beam diameter of ~30 μm was used to sputter the carbon-coated sample surface and to produce secondary ions. A mass resolution of ~6,000 was used to separate the $^{16}OH^-$ peak from the $^{17}O^-$. Typical errors in individual measurements were 0.5 to 1‰ (1σ). San Carlos olivine ($\delta^{18}O$ = +5.25‰; Eiler et al. 1995) was used as standard. Because matrix effects were neither monitored nor corrected, errors parallel to the fractionation line could be larger than stated below.

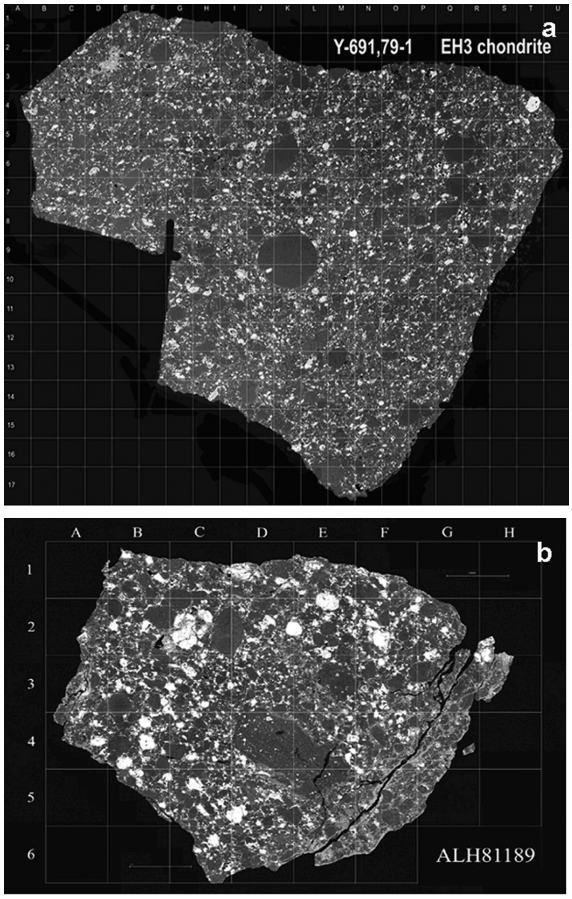

Fig. 1. Mosaics of backscattered electron (BSE) images of EH3 chondrites. In both image grids, each square is 1 mm^2. a) Thin section Y691,79-1. The largest chondrule in the center (J10) is partially surrounded by a rind of clastic matrix. The whole-rock exhibits a petrofabric: chondrules, chondrule fragments, and opaque assemblages are preferentially aligned in a NE-SW direction. The fabric is most prominent on the right and left sides of the image and less obvious in the central regions. b) Thin section ALH 81189,7. The largest chondrule (D4) (below center) is almost completely surrounded by a rind of clastic matrix. The whole-rock exhibits a petrofabric, silicate grains are aligned in a NW-SE direction.

RESULTS

Whole-Rock Petrofabric

The Y-691 whole rock exhibits a petrofabric running NE-SW in Fig. 1a. Chondrules, chondrule fragments, elongated

silicate grains, and opaque assemblages in the whole rock tend to be preferentially aligned. The petrofabric is identifiable on the right and left sides of the section, but is less obvious in the center. The mean azimuth of the 45 measured ≥0.5 mm size non-circular silicate particles in thin section Y691,79-1 is 71° ± 34º. The mean deviation of the silicate particles from the mean azimuth is 28º ± 28º. About half of the silicate particles (51%) have their long axes oriented to within 20º of the mean azimuth. The six chondrules and chondrule fragments with the highest aspect ratios (b/a > 2) tend to have small deviations from the mean azimuth (averaging 11º ± 11º), indicating a moderate preferred alignment.

Although ALH 81189 also appears to have a petrofabric (NW-SE; Fig. 1b), only seven silicate particles (chondrules) in the ALH81189,7 thin section exceed 0.5 mm in maximum dimension. The mean azimuth of the seven chondrules is 309º ± 25º. The mean deviation of these chondrules from the mean azimuth is 16º ± 18º. The largest chondrule (D4), which also has the highest aspect ratio (b/a = 2.4), has a deviation of 8º from the mean azimuth. (The ALH81189,7 section is about six times smaller in area than the Y-691,79-1 section, consistent with the smaller number of ≥0.5 mm sized chondrules in ALH81189,7.)

Petrography and Modal Abundance of Matrix Material

The material within the patches in Y-691 and ALH 81189 is dubbed "clastic matrix" because it contains relatively coarse (~2–20 μm size) angular fragments of mineral grains. These objects were presumably derived from crushed chondrules and opaque assemblages. Approximately 30 vol% of patch J10 in Y-691 (Figs. 2a and 2b) consists of silicate particles, ~25 vol% consists of opaque particles, and ~45 vol% is inferred to be composed of nebular fines. In ALH 81189, ~20 vol% of patch D4 consists of silicate particles, ~30 vol% consists of opaque particles, and ~50 vol% is inferred to be composed of nebular fines.

We determined the modal abundances of clastic matrix in the Y691,79-1 section to be 4.9 ± 0.5 vol% (111/2259 points) and that in ALH81189,7 to be 11.7 ± 1.2 vol% (99/847 points). The value in ALH 81189 is comparable to the 14 ± 5 vol% modal abundance of matrix determined by Huss and Lewis (1995) for a thin section of EH3 Qingzhen (and approximately reproduced by G. R. Huss (2008), on a different thin section of Qingzhen). The matrix abundance in Y-691 appears to be anomalously low.

Numerous patches of clastic matrix are present throughout Y-691 and ALH 81189, ranging up to ~700 μm in size. The patches occur in a variety of locations. Some are around chondrules and chondrule fragments, in some cases filling depressions ("craters") at the chondrule surface (Figs. 2a and 2b). Some matrix patches are adjacent to opaque assemblages (Fig. 2c). The shapes of the patches of clastic matrix are commonly governed by the shapes of the adjacent coarse constituents (i.e., chondrules, chondrule fragments and opaque assemblages).

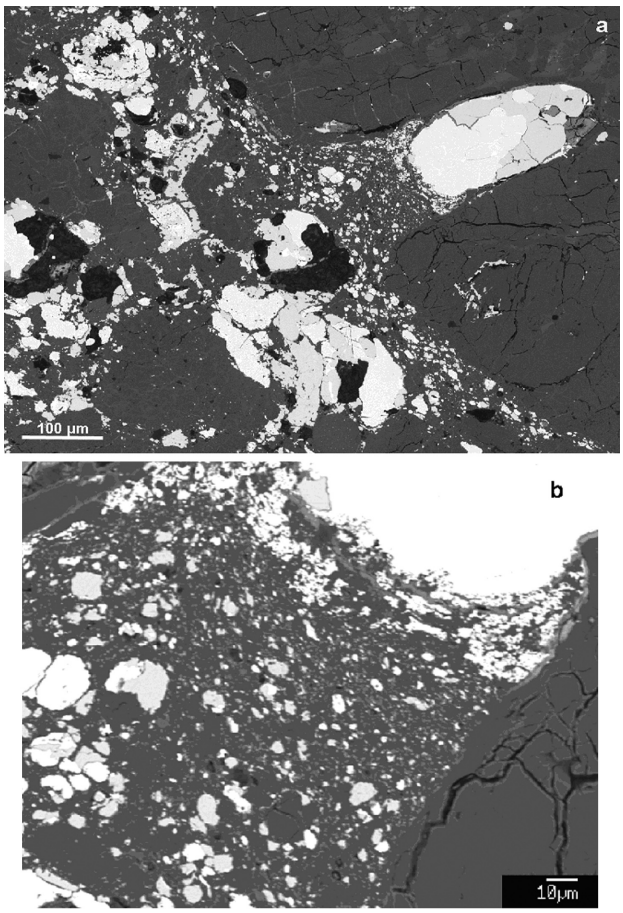

Fig. 2. Patches of clastic matrix in Y-691 (BSE images). a) Patch J10. The clastic matrix forms a thin rind partially surrounding the chondrule (right side) and fills a depression at the chondrule surface where it occurs adjacent to a large metal-sulfide assemblage. The clastic matrix patch contains numerous relatively coarse grains of metal and sulfide. b) Higher-magnification view of patch J10 filling the depression at the chondrule surface. The large metal-sulfide assemblage from Fig. 2a is at upper right. Numerous relatively coarse gains of metal, sulfide, phosphide and silicide (white and light gray grains) occur in the clastic matrix. Relatively coarse silicate grains (dark gray) also occur. The dark-gray-colored regions in between the coarse opaque grains are dominated by a fine-grained component, inferred to be nebular in origin and consisting of submicrometer-size grains. c) Clastic matrix patch H13 occurs between two opaque assemblages consisting mainly of metal and sulfide.

Some prominent examples of clastic matrix patches in thin section Y691,79-1 are described below.

Chondrule J10 is a very large ellipsoidal 3900 × 4500 μm size low-FeO porphyritic pyroxene-olivine (PPO) chondrule (Fig. 1a) partially surrounded (~300° of arc) by a discontinuous 5–82 μm thick rind of clastic matrix with an average thickness of ~50 μm (Figs. 2a and 2b). A depression at the chondrule surface is filled with a 120 × 245 μm ellipsoidal opaque assemblage and an overlying 130 × 160 μm patch of clastic matrix that is contiguous with the

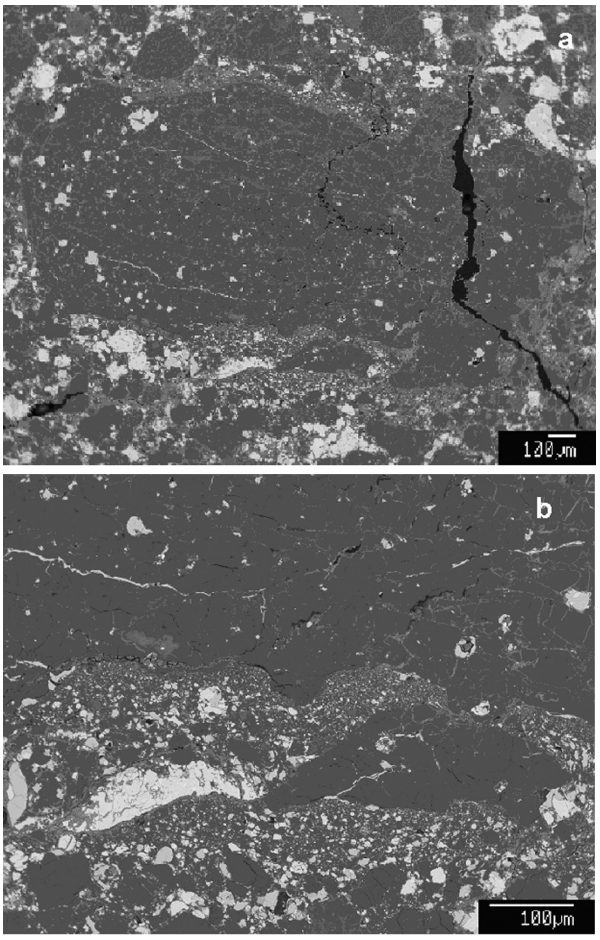

Fig. 3. Clastic matrix in ALH 81189, BSE images. a) Chondrule D4, the largest chondrule in the thin section, is nearly completely surrounded by clastic matrix. b) High-magnification view of the clastic matrix rind near the bottom of chondrule D4. The matrix near the chondrule surface contains fewer relatively coarse grains of opaque phases and silicates than clastic matrix regions away from the chondrule.

rind that partially surrounds the chondrule. (Chondrule J10 is larger than any of the chondrules from EH3 Qingzhen measured by Rubin and Grossman (1987). Separated chondrules in that study range up to 3400 µm in diameter; chondrules measured in thin section in that study have apparent diameters ranging up to ~1770 µm.)

Chondrule R5 is an ellipsoidal 1090 × 1210 µm size low-FeO porphyritic pyroxene (PP) chondrule that contains two depressions (80 × 190 µm and 50 × 390 µm) at opposite ends of the chondrule. Each is filled with clastic matrix.

Clastic matrix patch H13 is ~65 µm wide and occurs between two opaque assemblages (Fig. 2c). It is contiguous with a 10–70 µm wide rind that nearly completely surrounds an adjacent 350 × 680 µm size low-FeO PP chondrule.

Clastic matrix patch K11 almost completely surrounds a wedge-shaped 110 × 550 µm size radial pyroxene (RP) chondrule fragment. The patch consists of two main portions (140 × 490 µm and 50 × 380 µm) that flank the chondrule fragment.

Clastic matrix patch J14 is adjacent to a 710 µm diameter PP chondrule. The main portion of the patch (25–140 × 550 µm) forms a rind of varying thickness at one side of the chondrule; the minor portion of the patch along the opposite side of the chondrule is wedge-shaped and 65 × 140 µm in size.

The largest patch of clastic matrix in section ALH81189,7 occurs around low-FeO barred pyroxene (BP) chondrule D4 (Figs. 3a and 3b). The patch surrounds ~90% of this elongated 980 × 2010 µm size chondrule and ranges in thickness from ~150 to ~800 µm.

Identifiable opaque phases in Y-691 clastic matrix include kamacite α-(Fe,Ni), schreibersite $(Fe,Ni)_3P$, perryite $(Ni,Fe)_5(Si,P)_2$, troilite (FeS), niningerite (Mg,Fe)S, oldhamite (CaS), caswellsilverite ($NaCrS_2$), and daubréelite ($FeCr_2S_4$); the latter phase forms exsolution lamellae within some troilite grains. Silicate grains within the clastic matrix patches include enstatite ($MgSiO_3$), albitic plagioclase ($NaAlSi_3O_8$), silica (SiO_2) and diopside ($CaMgSi_2O_6$). These opaque and silicate phases are common minerals that occur in chondrules and coarse opaque assemblages throughout the meteorite.

Relatively coarse grains within matrix patches in ALH 81189 include common opaques (kamacite, schreibersite, perryite and troilite) and silicates (enstatite, forsterite (Mg_2SiO_4) and silica).

Most of the relatively coarse grains in the Y-691 matrix patches are irregular in shape and have ragged outlines (e.g., Fig. 2b). Approximately one third of the grains are relatively equant; most grains are elongated and have aspect ratios ranging from ~1.4 to 4. There is a tendency for these elongated grains to be aligned with the petrofabric of the whole rock. A small proportion (5–10%) of the grains within the clastic matrix patches are rounded or subhedral.

In Y-691 matrix patch J10 we determined the size-frequency distribution of 262 microscopically recognizable particles ranging in size from 0.6 to 32 µm (Fig. 4). Phi units (φ) are defined by the relationship $\varphi = -\log_2 d$ where d is the average apparent diameter of the particle in millimeters. Opaque particles have a smaller mean size (9.3 ± 1.4 φ; 1.6 (+2.6, –1.0) µm; n = 213) than silicate particles (8.0 ± 0.8 φ; 4.4 (+2.4, –2.2) µm; n = 49). The silicate particles have a roughly log-normal distribution, but the opaque particles have a large peak at 10–11 φ units, at the small-size extreme of the distribution. This suggests that numerous additional submicrometer-size opaque particles remain uncounted.

In addition to these clastic particles, there is an interstitial fine-grained, submicrometer component (hereafter "matrix fines") (e.g., Figs. 2b, 3b) that constitutes ~45 vol% of the clastic matrix in Y-691 and ~50 vol% in ALH 81189. This component is inferred to consist largely of nebular dust. If our values are correct for the modal abundances of clastic matrix

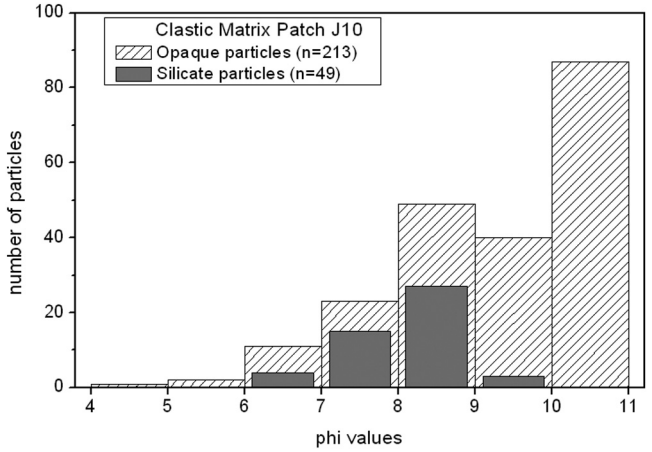

Fig. 4. Size-frequency distributions of 213 opaque particles and 49 silicate particles in matrix patch J10 of Y-691. The silicate particle distribution is approximately log normal. If it is assumed that the opaque particle distribution is approximately log normal, then the large peak at right indicates that many smaller opaque grains have not been counted.

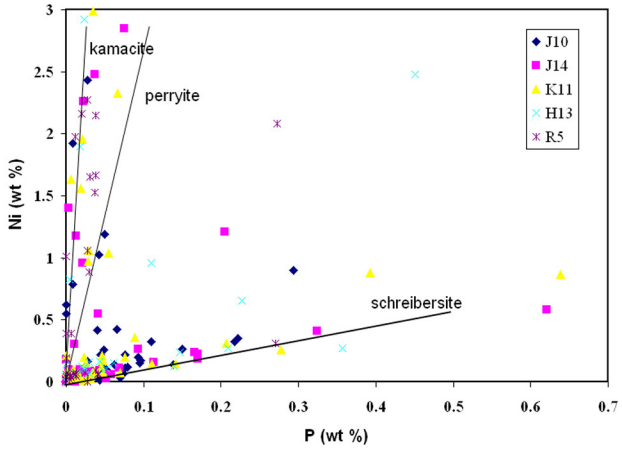

Fig. 5. Nickel versus P diagram for all five analyzed matrix patches using the complete data set of Y-691 (although some points lie beyond the limits of the diagram and are not plotted). Points that lie along the kamacite, perryite and schreibersite trends reflect analyses dominated by coarse grains derived from fragmented chondrules and opaque assemblages.

in Y-691 and ALH 81189, then matrix fines constitute ~2 vol% of Y-691 and ~5 vol% of ALH 81189.

Bulk Composition of Clastic Matrix Patches

A large fraction of the 3 μm wide analysis points in the matrix-grid regions in Y-691 and ALH 81189 overlap relatively coarse mineral grains. The compositional contributions of these grains are evident in some of the element-element diagrams; for illustrative purposes we use those in Y-691 (e.g., Fig. 5). Some data points are roughly aligned with expected mineral trends, reflecting different admixtures of matrix with these minerals. (The trend lines are based on the compositions of phases within opaque mineral fragments in Y-691 [Tables 1 and 2 of Kimura 1988].)

To assess the bulk compositions of matrix fines we developed screening criteria that were used to remove anomalous points from the grid arrays. The intent was to minimize compositional contributions from the relatively coarse non-nebular grains in the clastic matrix. The limits were chosen to omit analyses that differed by more than approximately 3 standard deviations from the means of the main compositional clusters. The same limits were applied to both chondrites.

We deleted points from the grids in both Y-691 and ALH 81189 that showed the following elemental concentrations (in wt%): Na > 3.0%; Mg < 4.5% or Mg >20.0%; Al > 3.0%; Si < 18% or Si > 32%; P > 0.6%; S < 1.05% or S > 8.0%; K < 0.10% or K > 0.45%; Ca > 2.0%; Cr > 0.40%; Mn > 0.45%; Fe < 2.5% or Fe > 33.5%; Co > 0.15%; Ni > 1.0%. For the elements P, K, Cr, Mn, Co, and Ni, if a value was outside the range, we discarded that value, not the entire analysis. We deleted analyses with totals <80 wt% or >102.5 wt%.

Altogether, 50% of the points (123/245) were eliminated in Y-691: 37–53% of the points were discarded in patches H13, J10, J14 and K11; 76% of the points were discarded in patch R5. In ALH 81189, 52% of the points (93/179) were eliminated: 36–52% of the points were discarded in patches B3, E4 and G2; 59–61% of the points were discarded in patches D4 and F3.

Within the restricted data set of Y-691 (Table 1), all five matrix patches are similar in bulk composition, differing mainly in their concentrations of Na (0.80–1.2 wt%) and K (0.14–0.26 wt%; Table 1). The restricted data set of ALH 81189 shows that matrix in this meteorite exhibits more inter-patch compositional variation; some patches differ appreciably in their bulk concentrations of Ca (0.57–0.90 wt%), Cr (0.14–0.25 wt%), Mn (0.17–0.28 wt%) and Ni (0.29–0.52 wt%) (Table 2). The average bulk compositions of matrix in Y-691 and ALH 81189 (all patches given equal weight) are listed in Table 3. These compositions are based on the restricted data sets and constitute the inferred nebular component.

Y-691

In comparing the compositions of the different matrix patches in Y-691, we omit clast-rich patch R5 in most of this discussion because its composition is represented by only 12 data points. Of the remaining four patches, K11 has the highest concentrations of Fe (10.4 wt%) and Ni (0.35 wt%), whereas J14 has the lowest concentrations of Fe (8.7 wt%) and Ni (0.20 wt%). The fine-grained fractions in patches H13, J14 and J10 have high concentrations of Na (1.2, 1.1, and 1.1 wt%, respectively) and K (0.25, 0.24, and 0.26 wt%, respectively), whereas matrix fines in patch K11 have the lowest Na and K (0.80 and 0.18 wt%, respectively).

Table 1. Inferred bulk compositions (wt%), standard deviations and 95% limits of the fine-grained portion of clastic matrix patches in Y-691 determined by electron microprobe analysis with a 3 μm wide beam.[a]

	H13 (n = 29)			J10 (n = 27)			J14 (n = 31)			K11 (n = 23)			R5 (n = 12)		
	Mean	Stdev	95%	Mean	Stdev	95%	Mean	Stdev	95%	Mean	Stdev	95%	Mean	Stdev	95%
Si	25.9	2.2	0.82	27.0	3.4	1.3	26.3	2.7	0.97	25.8	3.1	1.3	24.3	3.5	2.2
Al	1.6	0.87	0.33	1.5	0.94	0.37	1.5	0.93	0.34	1.4	0.74	0.32	1.0	0.50	0.31
Cr	0.16	0.06	0.02	0.17	0.07	0.03	0.08	0.04	0.03	0.17	0.10	0.04	0.16	0.17	0.04
Fe	9.5	4.4	1.7	9.7	6.4	2.5	8.7	6.4	2.4	10.4	6.1	2.6	9.5	6.6	4.1
Mn	0.05	0.03	0.01	0.08	0.04	0.02	0.06	0.05	0.02	0.06	0.04	0.02	0.11	0.12	0.08
Mg	11.0	3.2	1.2	10.9	2.8	1.1	13.2	3.1	1.1	11.8	3.2	1.4	11.8	3.9	2.5
Ca	0.52	0.13	0.05	0.60	0.41	0.16	0.59	0.37	0.14	0.64	0.42	0.18	0.44	0.27	0.17
Na	1.2	0.50	0.19	1.1	0.51	0.20	1.1	0.51	0.19	0.80	0.34	0.15	0.82	0.43	0.27
K	0.25	0.08	0.03	0.26	0.10	0.04	0.24	0.07	0.03	0.18	0.06	0.03	0.14	0.04	0.02
Ni	0.17	0.13	0.05	0.17	0.20	0.08	0.20	0.28	0.10	0.24	0.29	0.12	0.10	0.12	0.08
P	0.09	0.11	0.04	0.06	0.07	0.03	0.06	0.08	0.03	0.07	0.09	0.04	<0.04		
S	3.0	1.9	0.71	3.6	1.6	0.64	3.1	1.6	0.58	3.3	1.8	0.76	3.4	2.0	1.2
O	37.0	2.7	1.0	39.7	5.5	2.2	39.4	4.0	1.4	37.5	3.7	1.6	36.3	4.8	3.1
Total	90.4			94.8			94.5			92.4			88.1		

[a]There were initially 49 points per patch. Data points were omitted if their totals were <80 wt% or >102.5 wt% or had the following elemental concentrations (in wt%): Na > 3.0%; Mg < 4.5% or Mg >20.0%; Al > 3.0%; Si < 18% or Si > 32%; P > 0.6%; S < 1.05% or S > 8.0%; K < 0.10% or K > 0.45%; Ca > 2.0%; Cr > 0.40%; Mn > 0.45%; Fe < 2.5% or Fe > 33.5%; Co > 0.15%; Ni > 1.0%. The omitted points (50% of the total points) contained coarse mineral grains derived from fragmented chondrules and opaque assemblages. Data for Cl, Ti, Co and Zn are not included in the table because most analyses are below the detection limit.

Table 2. Inferred bulk compositions (wt%), standard deviations and 95% limits of the fine-grained portion of clastic matrix patches in ALH 81189 determined by electron microprobe analysis with a 3 μm wide beam.[a]

	B3 (n = 16)			D4 (n = 20)			E4 (n = 21)			F3 (n = 11)			G2 (n = 18)		
	Mean	Stdev	95%	Mean	Stdev	95%	Mean	Stdev	95%	Mean	Stdev	95%	Mean	Stdev	95%
Si	23.6	3.1	1.6	22.0	2.9	1.4	21.7	2.3	1.0	24.7	2.6	1.7	22.1	3.0	1.5
Al	1.1	0.47	0.25	1.3	0.51	0.24	1.2	0.34	0.15	0.94	0.49	0.33	1.2	0.32	0.16
Cr	0.14	0.10	0.05	0.24	0.10	0.05	0.25	0.08	0.04	0.19	0.10	0.07	0.20	0.09	0.04
Fe	12.5	6.5	3.4	14.6	6.4	3.0	14.0	3.4	1.5	11.6	5.0	3.3	12.7	3.7	1.8
Mn	0.22	0.11	0.06	0.28	0.05	0.02	0.21	0.07	0.03	0.28	0.19	0.13	0.17	0.06	0.03
Mg	12.5	4.5	2.4	12.3	3.0	1.4	12.1	2.2	1.0	11.8	4.4	2.9	12.7	3.5	1.7
Ca	0.57	0.32	0.17	0.90	0.37	0.17	0.65	0.17	0.08	0.62	0.38	0.25	0.71	0.25	0.12
Na	1.1	0.45	0.24	1.0	0.31	0.15	1.0	0.21	0.10	0.92	0.55	0.36	0.98	0.24	0.12
K	0.18	0.06	0.03	0.17	0.04	0.02	0.18	0.04	0.02	0.15	0.05	0.03	0.20	0.05	0.02
Ni	0.29	0.21	0.11	0.37	0.18	0.08	0.52	0.19	0.09	0.31	0.14	0.09	0.29	0.17	0.08
P	0.04	0.03	0.02	0.07	0.11	0.05	0.05	0.02	0.01	<0.04			0.05	0.04	0.02
S	4.1	1.7	0.90	5.8	1.8	0.84	5.2	1.2	0.54	4.2	1.6	1.1	5.1	2.0	0.99
O	40.5	4.6	2.4	37.8	4.4	2.0	38.3	2.3	1.0	40.0	3.7	2.5	38.6	4.0	2.0
Total	96.8			96.8			95.4			95.7			95.0		

[a]Data points were omitted using the same criteria listed in Table 1 for clastic matrix patches in Y-691. The omitted points contained coarse mineral grains derived from fragmented chondrules and opaque assemblages. The numbers of original data points in the different patches were B3 (30 points), D4 (49 points), E4 (44 points), F3 (28 points), and G2 (28 points). Altogether, 52% of the points were omitted. Data for Cl, Ti, Co and Zn are not included in the table because most analyses are below the detection limit.

Table 3. Bulk composition (wt%) of fine-grained silicate-rich matrix material in a few chondrite groups.[a]

	EH3	LL3	CR2	
Ref.	1	2	3	4
Si	25.1	22.8	19.7	13.3
Al	1.4	1.1	2.5	1.0
Cr	0.15	0.20	0.18	0.23
Fe	9.6	13.1	21.9	24.6
Mn	0.07	0.23	0.12	0.15
Mg	11.7	12.3	7.7	9.7
Ca	0.56	0.69	0.79	0.54
Na	1.0	1.0	1.8	0.59
K	0.21	0.18	0.56	0.10
Ni	0.18	0.36	0.30	n.d.
P	0.06	0.05	0.10	n.d.
S	3.3	4.9	0.90	3.4
O	38.0	39.0	35.9	30.1
Total	91.3	95.9	92.4	83.7
Concentration ratios relative to CI				
Ca/Al	0.37	0.59	0.30	0.50
Na/Al	1.25	1.60	1.26	1.04
Fe/Mg	0.44	0.57	1.51	1.35
Si/Mg	1.99	1.71	2.37	1.27
Cr/Mn	1.57	0.64	1.10	1.12
Na/K	0.58	0.68	0.39	0.72
Fe/S	0.94	0.87	7.90	2.35
Fe/Ni	3.22	2.20	4.41	–

[a]Matrix analyses from the literature were recalculated to list O as a separate component. The Fe-Ni metal in the Semarkona matrix analysis was recalculated assuming an Fe/Ni ratio of 10:1. The CI data are from Wasson and Kallemeyn (1988). n.d. = not determined. References: 1 = EH3 Y-691 (this study); 2 = EH3 ALH 81189 (this study); 3 = LL3.0 Semarkona (Huss et al. 1981); 4 = CR2 LAP 02342 (Wasson and Rubin 2009).

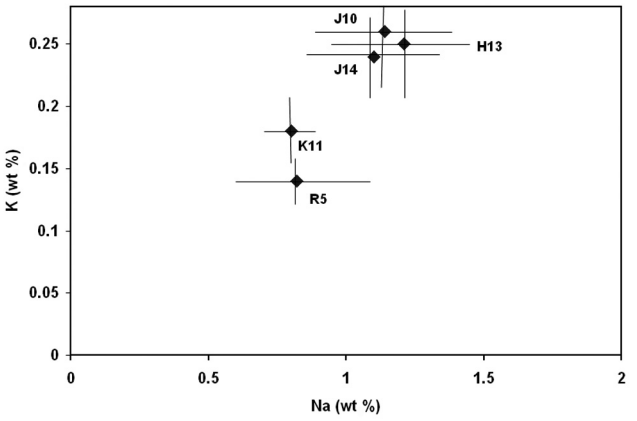

Fig. 6. Differences in the composition of K and Na in the fine-grained nebular component (i.e., matrix fines) among the different clastic matrix patches in Y-691. The patches form two clusters with essentially non-overlapping concentrations. The vertical and horizontal lines (i.e., the error bars) represent 95% confidence limits.

Among the clastic matrix patches in Y-691 only the alkali contents differ significantly (Fig. 6). The data form two clusters (J10-J14-H13 and K11-R5) that have non-overlapping concentrations of both Na and K at 95% confidence-level limits (determined using Student's t distribution for a two-sided test): e.g., patch H13, n = 29: 1.21 ± 0.19% Na, 0.25 ± 0.03% K; patch K11, n = 23: 0.80 ± 0.15% Na, 0.18 ± 0.03% K.

In order to show the differences between the matrix fines in H13 and K11, only analyses from the restricted data set are plotted in Figs. 7 and 8. Consistent with the alkali component in the fines being nebular, the trends do not lie along the lines expected for coarse-grained alkali-bearing phases—plagioclase, roedderite [$(K,Na)_2Mg_5Si_{12}O_{30}$], and djerfisherite [$K_6Na_9(Fe,Cu)_{24}S_{26}Cl$]. The K-Na diagram (Fig. 7a) shows a strong trend that has a much steeper slope (i.e., it is much more potassic) than plagioclase (which in Y-691 has a K/Na ratio of 0.01; Kimura 1988). The points also lie appreciably below the trend lines for roedderite (a rare phase in Y-691, present mainly as silicate inclusions in opaque assemblages, and which has a K/Na ratio of 1.3; Okada et al. 1975; Kimura 1988) and djerfisherite (which in Y-691 has a K/Na ratio of 4.1–7.0; El Goresy et al. 1986, 1988). Even though matrix patch H13 is richer in both Na and K than K11, both sets of points lie approximately along the same trend. This suggests that they contain different proportions of the same alkali-bearing component.

The Na-Al and K-Al diagrams (Figs. 7b and 7c) show that K11 tends to have lower Na and K concentrations than H13, particularly at high Al concentrations. H13 lies fairly close to the EH line in the Na-Al diagram (Fig. 7b).

Figure 8 is an abundance diagram showing the Mg- and EH-normalized bulk compositions of matrix fines in patches H13 and K11. The components are very similar in their abundances of most elements, differing mainly (by about 30%) in K and Na.

ALH 81189

In comparing the compositions of the different matrix patches in ALH 81189, we omit patch F3 because it is represented by only 11 data points (Table 2). In the remaining four matrix patches, elements that show large variations in concentration include Ca (0.17–0.90 wt%), Cr (0.14–0.25 wt%), Mn (0.17–0.28 wt%), and Ni (0.29–0.52 wt%) (e.g., Fig. 9a).

Differences in elemental concentrations in the fine-grained component in the different matrix patches are evident in the Ca versus Cr diagram (Fig. 9b). Patches F3 and G2 are similar in composition, but E4 is appreciably richer in Cr and B3 is somewhat poorer in Cr than F3 and G2. Whereas four of the patches have similar Ca concentrations, D4 is richer in Ca. The five patches form four "clusters" with little compositional overlap on the diagram.

The K-Na diagram for matrix in ALH 81189 (Fig. 9c) shows a similar trend to that of Y-691 matrix (Fig. 7a). In each case, the trend has a much steeper slope than plagioclase and a much shallower slope than either roedderite or djerfisherite.

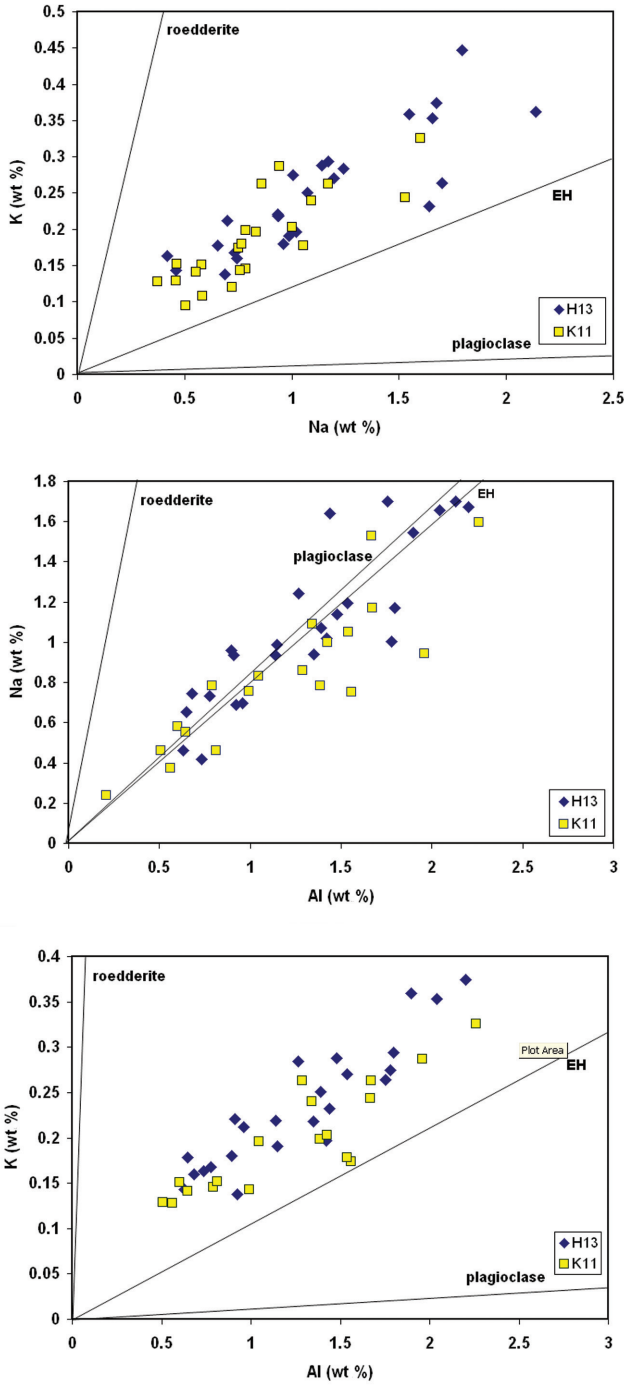

Fig. 7. Element-element plots with the restricted data set of Y-691 (Table 1) comparing the compositions of matrix fines in two matrix patches: H13 and K11. a) K versus Na. The points do not lie along the plagioclase or roedderite mineral trend lines. Although the H13 and K11 points lie approximately along the same trend as each other, the H13 distribution is richer in both Na and K. The EH-chondrite whole-rock K/Na ratio line is shown for reference. b) Na versus Al. The plagioclase line is very similar in Na/Al ratio to mean EH chondrites. c) K versus Al. The distributions do not lie along the plagioclase or roedderite mineral trend lines. Three points from patch K11 that had anomalously high ratios of both Al/Na and Al/K were omitted from diagrams 7b and 7c.

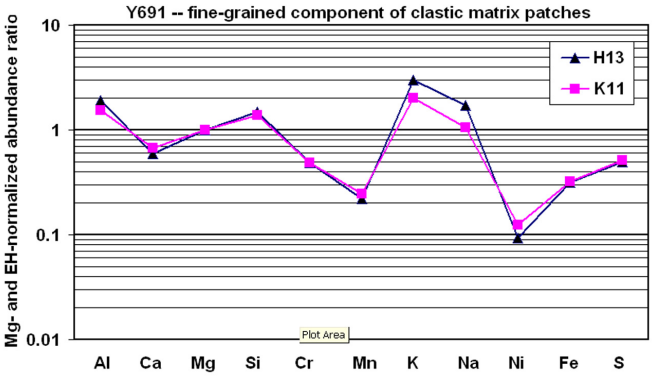

Fig. 8. Abundance diagram comparing the compositions of the fine-grained components of clastic matrix patches H13 and K11 in Y-691. Data are normalized to Mg and to mean EH chondrites (data from Wasson and Kallemeyn 1988). Elements are divided into "lithophiles" at the left and siderophiles and chalcophiles at the right. (However, in enstatite chondrites, many of the elements that are lithophile under more oxidizing conditions [e.g., Na, Mg, K, Ca, Cr, Mn] behave to some extent as chalcophiles.) For each set of elements, the species are ordered left to right on the basis of increasing volatility. Matrix fines in patches H13 and K11 exhibit similar inter-element trends but show differences in K and Na.

It seems clear that fine-grained matrix in both Y-691 and ALH 81189 contains the same nebular alkali component.

The fine-grained inferred nebular components of matrix in Y-691 and ALH 81189 are very similar. The principal differences are in two minor elements: Mn and, to a lesser extent, Ni; both elements have higher concentrations in ALH 81189 (Fig. 10).

Oxygen Isotopic Composition of Matrix Material in Y-691

The oxygen-isotopic compositions of clastic matrix patches in Y-691 are indistinguishable from those of olivine and pyroxene grains in adjacent chondrules (Table 4). The averages and standard deviations of ^{17}O values (in ‰) are 0.7 ± 0.5 and 0.0 ± 1.1 for chondrules and clastic matrix, respectively (Fig. 11). Within the uncertainties, both sets of objects lie on the terrestrial fractionation (TF) line on the standard three-isotope diagram.

DISCUSSION

Petrofabric

Foliations have been identified in numerous chondrite groups including CV3, OC, CR2, CM2.0 (i.e., CM1) and EL3 chondrites (e.g., Dodd 1965; Martin and Mills 1980; Cain et al. 1986; Sneyd et al. 1988; Scott et al. 1992; Zolensky et al. 1997; Rubin et al. 2007). The preferred orientations of chondrules, chondrule fragments and opaque assemblages in Y-691 and of chondrules in ALH 81189 constitute the first report of foliations in EH3 chondrites.

Table 4. Oxygen-isotopic compositions (‰) of matrix patches and olivine and pyroxene grains in adjacent chondrules in Y-691 as determined by the Cameca 7f GEO ion microprobe.

Patch	Host	Phase	^{18}O	1σ	^{17}O	1σ	^{17}O	1σ
J10	Matrix		4.8	1.0	1.0	1.0	–1.5	1.1
			4.0	0.9	0.9	0.9	–1.1	1.0
	Chondrules	Pyroxene	6.3	0.5	4.5	0.4	1.2	0.6
			5.2	0.5	3.8	0.3	1.1	0.6
			2.2	0.3	2.2	0.5	1.1	0.4
			4.6	0.6	2.6	0.3	0.2	0.6
			3.1	0.6	3.0	0.4	1.4	0.6
			4.0	0.5	3.4	0.6	1.3	0.6
			3.7	0.5	2.1	0.4	0.2	0.6
			0.6	0.5	0.0	0.5	–0.3	0.5
			5.8	0.6	3.5	0.5	0.4	0.7
			5.7	0.6	3.7	0.3	0.7	0.6
		Olivine	3.3	0.5	2.3	0.6	0.6	0.5
			3.9	0.6	3.0	0.5	1.0	0.6
R5	Matrix		4.2	1.1	3.9	0.5	1.8	1.1
	Chondrules	Pyroxene	7.4	0.6	5.2	0.4	1.4	0.6
J14	Matrix		1.9	0.8	0.8	0.5	–0.2	0.8
			6.5	0.8	4.9	0.4	1.5	0.8
	Chondrules	Pyroxene	5.6	0.5	2.9	0.5	0.0	0.6
			3.1	0.4	2.2	0.5	0.6	0.5
K11	Matrix		0.2	0.4	0.5	0.7	0.3	0.6
			–1.3	0.8	–0.6	0.5	0.1	0.8
			3.2	0.7	2.1	0.6	0.4	0.7
	Chondrules	Pyroxene	2.4	0.5	1.8	0.5	0.5	0.6
			5.6	0.7	3.9	0.6	1.0	0.8
			3.3	0.6	3.2	0.3	1.5	0.6
H13	Matrix		3.4	0.7	0.8	0.7	–1.0	0.8
	Chondrules	Pyroxene	3.8	0.4	1.9	0.4	–0.1	0.5

The most likely mechanism for producing foliations in chondrites, including Y-691 and ALH 81189 (Figs. 1a and 1b), is shearing caused by shock processes (e.g., Sneyd et al. 1988). It seems likely that chondritic materials were originally highly porous and easy to deform. Chondrules, chondrule fragments and opaque assemblages located adjacent to low-strength matrix material rotated and reoriented in response to shear, thereby producing a whole-rock petrofabric.

Low Totals of Matrix Analyses

Mean analytical totals for the different matrix patches in the restricted data set of Y-691 (Table 1) range from ~88 to 95 wt%; those in ALH 81189 range from ~95 to 97 wt%. Moderately low totals could be caused by any combination of plucking due to thin-section preparation, unanalyzed carbon-rich phases, water of hydration, and inherent porosity. The apparent absence of phyllosilicates in the matrix regions of Y-691 and ALH 81189 indicates that this material does not contain abundant water; thus, water of hydration is unlikely to be mainly responsible for the low analytical totals. The granular nature of the fine-grained matrix material indicates that there is some inherent porosity which is probably responsible for a large part of the low analytical totals. The lower analytical totals in Y-691 matrix may indicate a somewhat higher porosity than in ALH 81189 matrix.

The analytical totals for matrix patches in the CR2 chondrite LAP 02342 are appreciably lower, i.e., ~73 to 87 wt% (Wasson and Rubin 2009). This presumably reflects a higher water content and/or higher porosity in CR2 matrix relative to EH3 matrix.

Origin of Coarse Grains in Matrix Material

Because the mineralogy of the relatively coarse opaque and silicate grains within the clastic matrix patches reflects a subset of the common minerals present in the whole rock, it seems likely that these grains were derived from fragmented chondrules and opaque assemblages. Chondrules can undergo fragmentation both in the solar nebula and within the parent asteroid. The fact that Y-691 and ALH 81189 exhibit petrofabrics plausibly attributable to shock suggests that parent-body shock processes may be responsible for much of the chondrule fragmentation.

Possible Origins of Compositional Differences Among Matrix Patches

The nebular precursors of matrix patches were probably porous clumpy mixtures of individual mineral grains and grain fragments, amorphous particles, and aggregates of particles and grains. Many of the constituent particles and grains of the precursor clumps most likely consisted largely of recondensed materials that had evaporated during previous chondrule heating events (Wasson 2008). After the formation of planetesimals and the first generation of asteroids, impact events compacted these porous assemblages, crushed the clumps and reduced the overall porosities to those now observed (e.g., Trigo-Rodríguez et al. 2006).

Different matrix patches in the CR2 chondrite LAP 02342 show resolvable differences in composition on plots of S-Fe, Mg-Si, K-Na and K-Al (Wasson and Rubin 2009). The compositional differences among matrix patches in ALH 81189 are resolvable for Ca, Cr, Mn and Ni. The variations among matrix patches in Y-691 are resolvable only for the alkalis Na and K (Figs. 6–8).

Compositional differences among individual matrix patches were probably largely inherited from their precursors (which may have been chondrules produced by low degrees of melting; Wasson and Rubin 2009). A minor fraction of the compositional differences among precursor clumps may have been caused by the incorporation into the clumps of chondrule mesostasis spray ejected from neighboring chondrules during heating episodes. Because these were stochastic processes, some nebular assemblages may have varied in composition to the same extent as chondrules.

Possible Alkali Components in EH3 Matrix

The average matrix compositions in Y-691 and ALH 81189 show higher concentrations of Na (1.0 and 1.0 wt%, respectively) and K (0.21 and 0.18 wt%, respectively) (Table 3) than EH whole rocks (0.68 and 0.08 wt%, respectively; Wasson and Kallemeyn 1988).The alkali enrichment in the matrix is plausibly due to recondensation of volatiles onto the nebular dust precursors of matrix material after loss of the alkalis from chondrules during heating.

As indicated above, the different matrix patches in Y-691 and ALH 81189 lie along approximately the same Na-K trend (Fig. 7a, 9c), indicating that they contain variable fractions of an alkali-rich component. The matrix regions in the two meteorites have K/Na ratios (0.21 and 0.18) that are 1.5–1.8 times higher than the whole rock (0.12; Table 3; Wasson and Kallemeyn 1988). Because K is more volatile than Na, this is consistent with nebular fines being enriched in materials volatilized during chondrule formation (Wasson 2008).

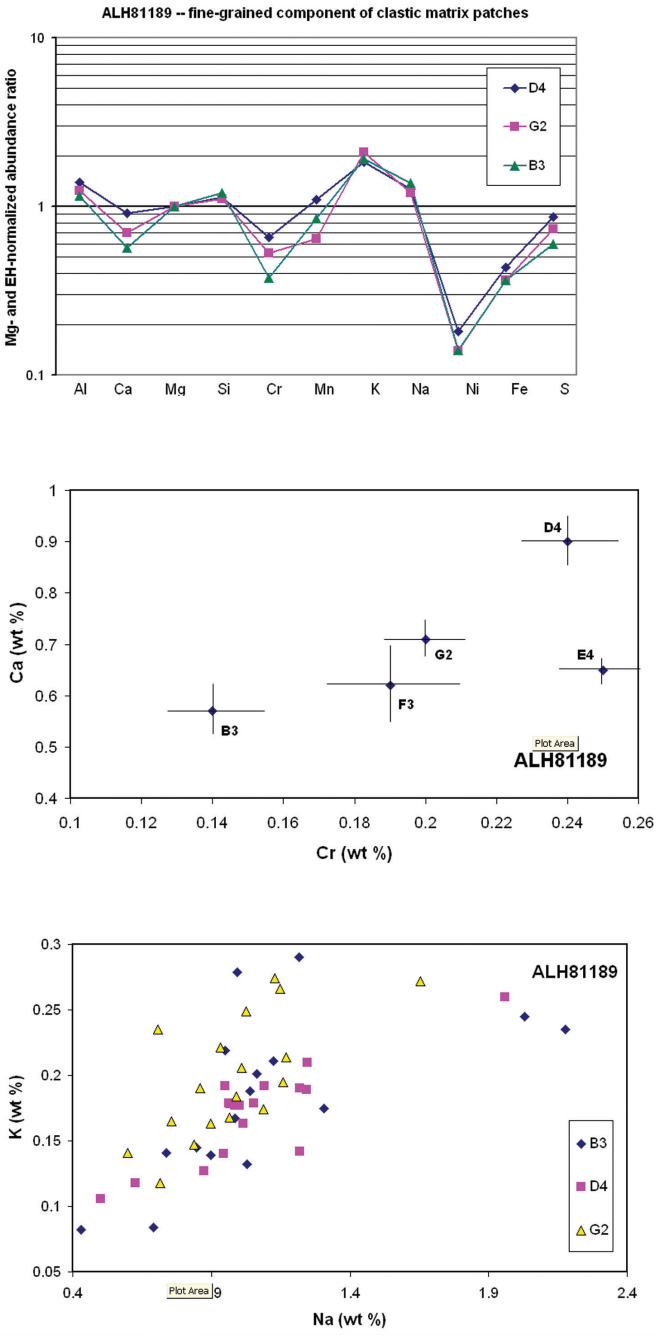

Fig. 9. Compositional comparisons among different matrix patches in ALH 81189. a) Abundance diagram comparing the compositions of the fine-grained components of clastic matrix patches D4, G2 and B3. Data are normalized to Mg and to mean EH chondrites. The patches differ in their bulk concentrations of Ca, Cr, Mn and Ni. b) Differences in the composition of Ca and Cr in the fine-grained nebular component among different clastic matrix patches. The patches form four "clusters" with little overlap in their elemental concentrations. The vertical and horizontal lines (i.e., the error bars) represent 95% confidence limits. c) K versus Na. The points show a strong positive correlation and lie approximately along the same trend as those in Y-691.

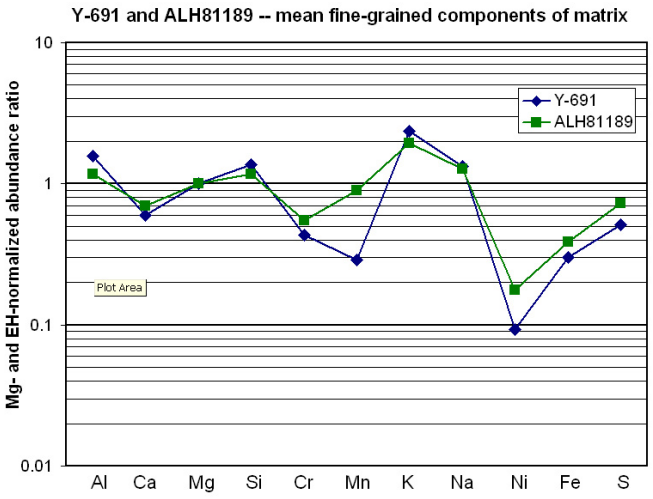

Fig. 10. Abundance diagram comparing the compositions of mean composition of fine-grained components of clastic matrix in Y-691 and ALH 81189. Data are normalized to Mg and to mean EH chondrites (data from Wasson and Kallemeyn 1988). The principal compositional differences are in Mn (0.07 ± 0.02 versus 0.23 ± 0.05 wt%) and Ni (0.18 ± 0.05 versus 0.36 ± 0.10 wt%); ALH 81189 matrix is richer in both elements.

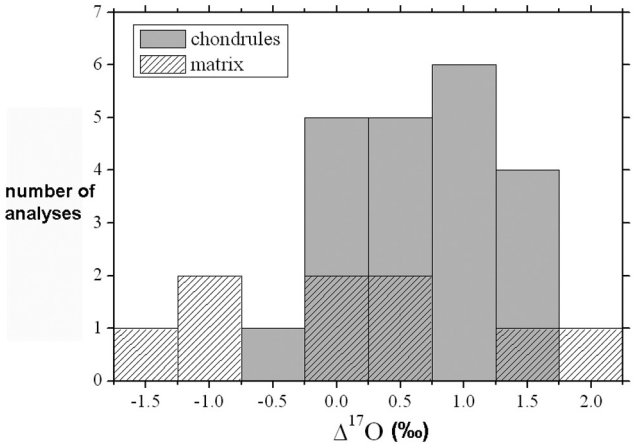

Fig. 11. A histogram showing $\Delta^{17}O$ values of chondrule olivine and pyroxene grains and clastic matrix patches from Y-691. The values of the patches encompass a somewhat wider range than those of chondrules. However, within the analytical uncertainty, there are no resolvable O-isotopic differences between chondrules and clastic matrix.

Implications of O-Isotopic Homogeneity

Previous studies have established that the bulk O-isotopic compositions of enstatite chondrites plot near the terrestrial mass-fractionation line (Clayton et al. 1976, 1984; Newton et al. 2000). Separated chondrules (Clayton et al. 1984) and SIMS analyses of silicate phases (Kimura et al. 2003) exhibit similar compositions. Our SIMS measurements on chondrule olivine and pyroxene and on clastic matrix patches in EH3 Y-691 agree with these general observations for the constituents of enstatite chondrites. These results imply that at the scale of an ion-probe spot (about 10 μm) all of these materials (chondrules, clastic matrix, and silicate grains derived from chondrules) originated from the same O-isotope reservoirs. (The sole exceptions appear to be (a) refractory inclusions in type-3 enstatite chondrites that have O-isotopic compositions similar to those of refractory inclusions in other chondrite groups (e.g., Guan et al. 2000; Fagan et al. 2001) and (b) presolar silicate grains that have similar O-isotopic compositions to those in other chondrite groups [Ebata et al. 2008; Yurimoto 2006].)

Modal Abundance of Matrix in EH3 Chondrites

Huss and Lewis (1995) reported the modal matrix abundance of EH3 Qingzhen to be 14 ± 5 vol% and that of EH4 Indarch to be ~10 vol%. They suggested that the lower abundance in Indarch resulted from metamorphic recrystallization. Although they could find no petrographic evidence of matrix in the Abee EH impact-melt breccia, Huss and Lewis (1995) assumed matrix abundances in both Indarch and Abee to be 12.5 ± 1.3 vol%. [In fact, matrix material has been destroyed in Abee, an impact-melt breccia (e.g., Rubin and Scott 1997).] Modal analyses of matrix in the Huss and Lewis paper were done microscopically by G. R. Huss using relatively low magnification (~200×) and a click-stop stage. Huss switched between reflected and transmitted light in order to distinguish matrix from chondrule fragments. G. R. Huss (personal communication, 2008) used this technique to make a modal analysis of a new section of Qingzhen (1339 points) and derived a value of 17.3 vol%, somewhat higher than the previous value. It is likely that Huss' estimate applies to what is termed here "clastic matrix."

Although our modal analyses of matrix in Y-691 and ALH 81189 were done at higher magnification (500×), we followed a similar methodology, switching between transmitted and reflected light. The lower-magnification technique used by Huss tends to include more points that land on small chondrule fragments than our higher-magnification technique, so his results would tend to yield higher estimates than ours of the modal abundance of matrix. Our value of ~12 vol% clastic matrix in ALH 81189 is in the same range as the analyses determined by Huss for Qingzhen. It thus appears that Y-691 has less clastic matrix material than other primitive EH3 chondrites.

Scenarios Explaining Differences in the Modal Abundance of Matrix among Chondrite Groups

Different chondrite groups have different abundances of fine-grained (nebular) matrix material but the actual values are uncertain because published modal matrix data have not generally been corrected for the presence of clastic and secondary materials. Including such non-nebular materials,

the matrix abundances (in vol%) among non-carbonaceous chondrites (i.e., among rocks minimally affected by aqueous alteration) are: EH3, 5–12% (our values); LL3 (Semarkona), 15%; R3 (ALH 85151), ~35%; (e.g., Huss et al. 1981; Rubin and Kallemeyn 1989; Brearley 1996; this study). The average chondrule abundances in these groups (in vol%) are EH (15–20%), H–L–LL (65–75%) and R (35%) (Table 1 of Rubin 2000). The chondrule/matrix modal-abundance ratio among the non-carbonaceous chondrites thus varies from ~1 to 5.

We offer two possible explanations for the differences among chondrite groups in the chondrule/matrix ratio:

1. There may have been differences in the efficiency of the chondrule-formation process (i.e., in the conversion of fine materials into chondrules). It seems likely that the intensity, duration and/or frequency of episodes of chondrule formation (e.g., transient heating events) varied from one nebular location to another. It is possible that these parameters varied with heliocentric distance and time. If EH chondrites have somewhat lower abundances of fine-grained nebular materials than other chondrite groups, then they may have experienced more episodes of chondrule formation, resulting in a paucity of dust available to agglomerate into chondrites in the EH region of the nebula. This scenario conflicts with the view that chondrule formation also produced fine materials, and that multiple melting cycles should have produced a steady-state chondrule/fines ratio (e.g., Wasson 2008).
2. There is little doubt that planetesimal formation occurred in the nebular midplane. Some fraction of finer-grained nebular materials may not have been agglomerated because they were suspended by turbulence in the gas above the midplane. The amount of gas turbulence in the nebula may have varied with time and/or with nebular location (e.g., Cuzzi and Weidenschilling 2006). If the fine-grained matrix abundance in EH3 chondrites is really as low as 2–5 vol%, this may indicate that EH chondrites formed in a nebular region of enhanced turbulence and diminished efficiency in the settling of fine-grained dust to the midplane. This explanation seems the more plausible of the two.

CONCLUSIONS

In the EH3 chondrites, clastic matrix constitutes ~5 vol% of Y-691 and ~12 vol% of ALH 81189. This material consists of approximately 25–30 vol% relatively coarse fragmental opaque grains and assemblages, 20–30 vol% silicate grain fragments, and 45–50 vol% of a fine-grained component (matrix fines) inferred to be nebular in origin. The low inferred abundance of fine-grained matrix abundance in EH3 chondrites (2–5 vol%) may indicate that EH chondrites formed in a nebular region of enhanced turbulence and diminished efficiency in the settling of fine-grained dust to the midplane. In contrast to observations of easily resolvable compositional differences among different matrix regions in the CR2 chondrite LAP 02342 (Wasson and Rubin 2009), those in ALH 81189 are only marginally resolvable in Ca, Cr, Mn, and Ni, and those in Y-691 show resolvable variations only in K and Na. The uniformity of O-isotopic compositions among different components of EH chondrites indicates that nebular fine-grained materials (the precursors of chondrules and matrix) had homogeneous O-isotopic compositions. The whole-rock petrofabrics in Y-691 and ALH 81189 were most likely produced by shock process on their parent asteroid.

Acknowledgments–We are grateful to the curators at the National Institute of Polar Research, Japan, for the loan of the thin section of Y-691 and permission to analyze it with the ion microprobe. We also thank the curators at NASA Johnson Space Center and the Antarctic Meteorite Working Group for the loan of a section of ALH 81189. We thank Y. Guan of Caltech for technical assistance with the ion probe, C. Lau of UCLA for his help in determining the petrofabrics, and G. R. Huss of the University of Hawai'i for discussions about (and generation of new data on) the abundance of matrix material in EH3 chondrites. We are grateful to M. Kimura and S. Ebata for their reviews of the manuscript. This work was supported in part by NASA grants NNG06GF95G (A. E. Rubin) and NNG06GG35G (J. T. Wasson), and Korea Science and Engineering Foundation (KOSEF) grant R01-2006-000-10522-0 (B.-G. Choi).

Editorial Handling—Dr. Allan Treiman

REFERENCES

Brearley A. J. 1996. Nature of matrix in unequilibrated chondrites and its possible relationship to chondrules. In *Chondrules and the protoplanetary disk*, edited by Hewins R. N., Jones R. H., Scott E. R. D. Cambridge: Cambridge University Press. pp. 137–151.

Cain P., McSween H. Y., and Woodward N. B. 1986. Structural deformation of the Leoville chondrite. *Earth and Planetary Science Letters* 77:165–175.

Clayton R. N., Onuma N. and Mayeda T. K. 1976. A classification of meteorites based on oxygen isotopes. *Earth and Planetary Science Letters* 30:10–18.

Clayton R. N., Mayeda T. K. and Rubin A. E. 1984. Oxygen isotopic compositions of enstatite chondrites and aubrites. Proceedings, 15th Lunar and Planetary Science Conference. pp. C245–C249.

Cuzzi J. N. and Weidenschilling S. J. 2006. Particle-gas dynamics and primary accretion. In *Meteorites and the early solar system II*, edited by Lauretta D. S. and McSween H. Y. Tucson: The University of Arizona Press. pp. 353–381.

Dodd R. T. 1965. Preferred orientation of chondrules in chondrites. *Icarus* 4:308–316.

Ebata S. and Yurimoto H. 2008. Identification of silicate and carbonaceous presolar grains in the type 3 enstatite chondrites. In *Origin of matter and evolution of galaxies*, edited by Suda T., Nozawa T., Ohnishi A., Kato K., Fujimoto M. Y., Kajino T., and Kubono S. Melville, New York: American Institute of Physics. pp. 412–414.

Ebata S., Nagashima K., Itoh S., Kobayashi S., Sakamoto N., Fagan T. J., and Yurimoto H. 2006. Presolar silicate grains in enstatite chondrites (abstract #1619). 37th Lunar and Planetary Science Conference. CD-ROM.

Ebata S., Fagan T. J. and Yurimoto H. 2007. Identification of silicate and carbonaceous presolar grains in the type 3 enstatite chondrite ALHA81189 (abstract). *Meteoritics & Planetary Science* 42: A38.

Ebata S., Fagan T. J. and Yurimoto H. 2008. Identification of silicate and carbonaceous presolar grains by SIMS in the type-3 enstatite chondrite ALHA81189. *Applied Surface Science* 255:1468–1471.

Eiler J. M., Farley K. A., Valley J. W., Stolper E. M., Hauri E. H., and Craig H. 1995. Oxygen isotope evidence against bulk recycled sediment in the mantle sources of Pitcairn Island lavas. *Nature* 377:138–141.

El Goresy A., Woolum D. S., Ehlers K., and Ivanov A. V. 1986. Planetary metamorphic events in unequilibrated EH chondrites (abstract). 17th Lunar and Planetary Science Conference. pp. 202–203.

El Goresy A., Yabuki H., Ehlers K., Woolum D. and Pernicka E. 1988. Qingzhen and Yamato-691: A tentative alphabet for the EH chondrites. *Proceedings of the NIPR Symposium on Antarctic Meteorites* 1:65–101.

Fagan T. J., McKeegan K. D., Krot A. N. and Keil K. 2001. Calcium-aluminum-rich inclusions in enstatite chondrites (II): Oxygen isotopes. *Meteoritics & Planetary Science* 36:223–230.

Guan Y., McKeegan K. D. and MacPherson G. J. 2000. Oxygen isotopes in calcium-aluminum-rich inclusions from enstatite chondrites: New evidence for a single CAI source in the solar nebula. *Earth and Planetary Science Letters* 181:271–277.

Huss G. R. and Lewis R. S. 1995. Presolar diamond, SiC, and graphite in primitive chondrites: Abundances as a function of meteorite class and petrologic type. *Geochimica et Cosmochimica Acta* 59: 115–160.

Huss G. R., Keil K., and Taylor G. J. 1981. The matrices of unequilibrated ordinary chondrites: Implications for the origin and history of chondrites. *Geochimica et Cosmochimica Acta* 45: 33–51.

Kallemeyn G. W., Rubin A. E. and Wasson J. T. 1996. The compositional classification of chondrites: VII. The R chondrite group. *Geochimica et Cosmochimica Acta* 60:2243–2256.

Kimura M. 1988. Origin of opaque minerals in an unequilibrated enstatite chondrite, Yamato-691. *Proceedings of the NIPR Symposium on Antarctic Meteorites* 1:51–64.

Kimura M., Hiyagon H., Lin Y. and Weisberg M. K. 2003. FeO-rich silicates in the Sahara 97159 (EH3) enstatite chondrite: Mineralogy, oxygen isotopic compositions, and origin. *Meteoritics & Planetary Science* 38:389–398.

Larimer J. W. and Bartholomay M. 1979. The role of carbon and oxygen in cosmic gases: some applications to the chemistry and mineralogy of enstatite chondrites. *Geochimica et Cosmochimica Acta* 43:1455–1466.

Lattimer J. M., Schramm D. N. and Grossman L. 1978. Condensation in supernova ejecta and isotopic anomalies in meteorites. *The Astrophysical Journal* 219:230–249.

Leshin L. A., Rubin A. E. and McKeegan K. D. 1997. The oxygen isotopic composition of olivine and pyroxene from CI chondrites. *Geochimica et Cosmochimica Acta* 61:835–845.

Martin P. M. and Mills A. A. 1980. Preferred orientations in meteorites. *Earth and Planetary Science Letters* 51:18–25.

Nagahara H. 1985) Petrology of enstatite chondrites, Y-691 (EH3) and Y-74370 (EH4) (abstract). *Proceedings of the NIPR Symposium on Antarctic Meteorites* 10:12–14.

Newton J., Franchi I. A. and Pillinger C. T. 2000. The oxygen-isotopic record in enstatite meteorites. *Meteoritics & Planetary Science* 35:689–698.

Okada A., Yagi K., and Shima M. 1975. Petrological studies of the Yamato meteorites part 2. Petrology of the Yamato meteorites. *Memoirs of National Institute of Polar Research* (Special Issue) 5:67–82.

Prinz M., Nehru C. E., Weisberg M. K., and Delaney J. S. 1984. Type 3 enstatite chondrites: A newly recognized group of unequilibrated enstatite chondrites (UECs) (abstract). 15th Lunar and Planetary Science Conference. pp. 653–654.

Rubin A. E. 1997. Sinoite (Si_2N_2O): Crystallization from EL chondrite impact melts. *American Mineralogist* 82:1001–1006.

Rubin A. E. 2000. Petrologic, geochemical and experimental constraints on models of chondrule formation. *Earth Science Reviews* 50:3–27.

Rubin A. E. and Grossman J. N. 1987. Size-frequency distributions of EH3 chondrules. *Meteoritics* 22:237–251.

Rubin A. E. and Kallemeyn G. W. 1989. Carlisle Lakes and Allan Hills 85151: Members of a new chondrite grouplet. *Geochimica et Cosmochimica Acta* 53:3035–3044.

Rubin A. E. and Scott E. R. D. 1997. Abee and related EH chondrite impact-melt breccias. *Geochimica et Cosmochimica Acta* 61: 425–435.

Rubin A. E., Wang D., Kallemeyn G. W. and Wasson J. T. 1988. The Ningqiang meteorite: Classification and petrology of an anomalous CV chondrite. *Meteoritics* 23:13–23.

Rubin A. E., Trigo-Rodríguez J. M., Huber H. and Wasson J. T. 2007. Progressive aqueous alteration of CM carbonaceous chondrites. *Geochimica et Cosmochimica Acta* 71:2361–2382.

Score R. and Mason B. 1984. Description of ALHA81189. *Antartctic Meteorites Newsletter* 7(2):1–29.

Scott E. R. D., Keil K. and Stöffler D. 1992. Shock metamorphism of carbonaceous chondrites. *Geochimica et Cosmochimica Acta* 56: 4281–4293.

Sneyd D. S., McSween H. Y., Sugiura N., Strangway D. W., and Nord G. L. 1988. Origin of petrofabrics and magnetic anisotropy in ordinary chondrites. *Meteoritics* 23:139–149.

Trigo-Rodríguez J. M., Rubin A. E. and Wasson J. T. 2006. Non-nebular origin of dark mantles around chondrules and inclusions in CM chondrites. *Geochimica et Cosmochimica Acta* 70:1271–1290.

Wasson J. T. 2008. Evaporation of nebular fines during chondrule formation. *Icarus* 195:895–907.

Wasson J. T. and Kallemeyn G. W. 1988. Compositions of chondrites. *Philosophical Transactions of the Royal Society of London A* 325:535–544.

Wasson J. T. and Rubin A. E. 2009. Composition of matrix in the CR chondrite LAP 02342. *Geochimica et Cosmochimica Acta* 73: 1436–1460.

Yurimoto H. 2006. Stardusts in meteorites—Precursors of planets. In *Origin of matter and evolution of galaxies*, edited by Kubono S., Aoki W., Kajino T., Motobayashi T., and Nomoto K. Melville, New York: American Institute of Physics. pp. 319–323.

Zolensky M. E., Mittlefehldt D. W., Lipschutz M. E., Wang M.-S., Clayton R. N., Mayeda T. K., Grady M. M., Pillinger C. T., and Barber D. 1997. CM chondrites exhibit the complete petrologic range from type 2 to 1. *Geochimica et Cosmochimica Acta* 61: 5099–5115.